Physics – Uspekhi **66** (1) 90 – 102 (2023)

METHODOLOGICAL NOTES PACS numbers: **71.36.+c**, 73.20.Mf, **78.68.+m**

Plasmon-polariton at the interface of a uniaxial crystal and a metal: real dispersion equation and its analysis

V I Alshits, V N Lyubimov

DOI: https://doi.org/10.3367/UFNe.2021.12.039122

Contents

Abstract. An analytical description of the plasmon polariton localized at the arbitrarily oriented interface of a uniaxial crystal and an isotropic metal is discussed. A compact real form of the general dispersion equation determining the basic wave properties is obtained. The solutions of this equation are analyzed for the particular orientations of the sagittal plane and interface. An approximate solution of the dispersion equation is developed on the basis of the iteration method, which has proved to be effective even for the general case of an arbitrary interface orientation. General relations of the theory are specified for a series of crystals.

Keywords: localized electromagnetic waves, polaritons in dielectrics, plasmons in metals, plasmon-polaritons at the crystal–metal interface, dispersion equation

1. Introduction

Electromagnetic waves in the optical range, localized at the interface of solid structures (polaritons in dielectrics or plasmons in metals), are much more selective concerning the conditions of their existence than is their acoustic counterpart, the Rayleigh wave. It is known that a surface elastic wave can propagate on the free boundary of any isotropic medium [1] and even on an arbitrary cut of any crystal, which is guaranteed by strict theorems [2]. At the same time, a surface polariton at the interface of any isotropic dielectric material (including the boundary with a vacuum) is strictly prohibited. More precisely, a 'dispersionless' polariton is forbidden at positive permittivity values of two media, virtually indifferent to its frequency. However, 'dispersive' polaritons can propagate in the vicinity of certain resonance frequencies, where one of the media changes the sign of its permittivity. Such polaritons have been actively studied [3–5] and are now widely used.

It might seem that the polariton 'locked' inside the medium of an isotropic dielectric with an ideally metallized surface is a close analog of a permanently existing elastic wave trapped in a solid. However, metallization not only fails to facilitate the propagation of the polariton, but, on the contrary, even 'kills' dispersive modes [6]. On the other hand, the same metallization of the surface of a uniaxial crystal [6] generates a specific dispersion-type polariton near the interface in the vicinity of the frequency where one of the permittivity values of the crystal becomes negative.

However, as has been shown by Dyakonov [7], the 'switching on' of anisotropy also rehabilitates dispersionless eigenmodes, i.e., surface polaritons, which can propagate at any frequency in a crystal with positive values of permittivity. To do this, a uniaxial crystal must make contact, not with an ideal metal, but with an isotropic dielectric whose permittivity falls in a certain range (see Section 3 for details). Study [7] explored the orientation of a crystal with an optical axis parallel to the interface. The region where a polariton exists turned out to be limited by a rather narrow sector of the optical axis directions in this plane. The generalization of [7] in [8, 9] for the case of an arbitrary orientation of the optical axis has shown that the extension of the polariton existence region is determined by an increase in crystal anisotropy (as in [7]) rather than by the deviation of the optical axis from the interface. The same limitation on the region where a polariton exists also occurs for the interface between an isotropic dielectric and a biaxial crystal [8, 10–12]. In optics, increasing the anisotropy is obviously a rather challenging task. How-

V I Alshits (*), **V N Lyubimov** (**)
Shubnikov Institute of Crystallography,
Federal Scientific Research Center Crystallography and Photonics,
Russian Academy of Sciences,
Leninskii prosp. 59, 119333 Moscow, Russian Federation
E-mail: (*) valshits@mail.ru, (**) lyubvn36@mail.ru

Received 29 September 2021, revised 19 November 2021
Uspekhi Fizicheskikh Nauk **193** (1) 96 – 109 (2023)
Translated by M Zh Shmatikov

ever, photonic crystals with anomalously large anisotropy are now available.

On the other hand, there is another, rather paradoxical, way to extend the region where dispersionless polaritons exist. To do this, instead of using the ideal metallization of the dielectric discussed above, it suffices to use a normal metal that allows an accompanying (usually highly localized) wave, a plasmon, to enter its interior. The resulting hybrid wave, a plasmon-polariton, turns out to be widely allowed and, most importantly, very popular in applications precisely because of the plasmon, which is extensively used in modern devices [13–18].

In this case, the dielectric can be either isotropic or anisotropic. The choice of a crystal is usually driven either by optimizing the free path of a plasmon-polariton on a suitable crystal cut [19–21] or by the possibility of exciting a plasmon in a metal by means of oblique incidence of the polariton on the interface in the crystal at an angle corresponding to total internal reflection [22–25]. In the latter case, the parameters are chosen in such a way that there is no reflected wave in the crystal, and the pumping of energy through the interface compensates absorption in the metal, thus maintaining stationary propagation of the plasmon in the metal with a constant amplitude.

The formal reason for facilitating the conditions for the existence of plasmon-polaritons is the universal negativity of the permittivity ε_{m} of the metal at any optical frequency. The same occurs to dispersive polaritons near resonance frequencies, where the sign of some of the permittivity values also changes. In both cases, changing the signs of the corresponding terms in the dispersion equation provides an extension of the range where its solutions exist. However, the plasmon-polariton, in contrast to the dispersive polariton, exists in a wide frequency range.

There is another important aspect related to dispersion equations in such problems, which arises when dealing with crystals. It is related to the well-known problem of optics and acoustics of anisotropic media, where the dispersion equation for one unknown real parameter (for example, the refractive index n) turns out to be complex, splitting into two, so the problem looks overdetermined. Strict theorems have long been proven (both in acoustics [26] and in optics [27]) that these two equations are analytically related and must have the same roots. Nevertheless, many authors avoid dealing with such complexities, preferring to consider symmetric crystal orientations when the dispersion equation turns out to be real [19, 20, 28–30]. The compact dispersion equation [28, 29], which corresponds to the Dyakonov geometry [7], is especially popular. However, to the best of the authors' knowledge, the general real dispersion equation for plasmon-polaritons at the uniaxial crystal–metal interface with an arbitrary orientation of the interface has not yet been derived. This deficiency is removed below.

After the necessary mathematical formulation of the problem in Section 2 and the derivation in Section 3 of the general complex dispersion equation, the latter is reduced to a compact real form. Verification shows that it transforms into well-known equations corresponding to particular cases of orientation when the optical axis of the crystal is parallel to the sagittal plane [30] or to the interface [28, 29] (Dyakonov's geometry). In the former case (Section 4), it can be easily solved exactly, but this solution requires a nontrivial analysis of the stability limits. In the latter case (Section 5), an iterative procedure for the approximate solution of the equation is proposed. Its efficiency is shown by a comparison with the numerical solution of the exact equation for a dozen crystals, including a superanisotropic photonic crystal, and the boundaries of the existence of the solution are analyzed. In Section 6, the iterative formalism developed is generalized to arbitrary orientation of the interface. Specific crystals are used as examples to show that the first iteration already provides a good accuracy of description with deviations from the exact numerical dependences of $\sim 2\%$. Section 7 summarizes the results of the study.

2. Plasmon-polariton propagation geometry and wave field parameters

In this study, we consider a natural electromagnetic wave localized at an arbitrarily oriented interface between an optically uniaxial crystal with permittivity values ε_{o} and ε_{e} and a metal with permittivity $\varepsilon_{\mathrm{m}} < 0$ and magnetic permeability $\mu_{\mathrm{m}} = 1$.

Figure 1 shows the geometric characteristics of the system. The arbitrary orientation of the interface plane is given by the unit normal vector $\mathbf{n}$, which also defines the coordinate axis y. The metal is located in the region $y \leqslant 0$, and the crystal, in the region $y \geqslant 0$. The direction of the optical axis of the crystal is characterized by a unit vector $\mathbf{c}$, which makes an arbitrary angle θ with the interface plane xz. For definiteness, the coordinate axis x is chosen along the projection of the optical axis $\mathbf{c}$ onto this plane. The direction of wave propagation along the interface is set by the unit vector $\mathbf{m}$ making angle φ with the x-axis. In terms of the vectors $\mathbf{m}$, $\mathbf{n}$, and $\mathbf{t} = \mathbf{m} \times \mathbf{n}$ defining the wave geometry, the vector $\mathbf{c}$ along the optical axis is equal to

$$\mathbf{c} = \mathbf{m}\cos\theta\cos\varphi + \mathbf{n}\sin\theta + \mathbf{t}\cos\theta\sin\varphi\,. \tag{1}$$

The electromagnetic field in the structure under consideration consists of two pairs of coupled partial waves in a crystal and an isotropic medium. In the crystal, these components are ordinary (o) and extraordinary (e) waves, and in the metal, they are waves with TM and TE polarizations. The total wave field propagating along the vector $\mathbf{m}$ (see

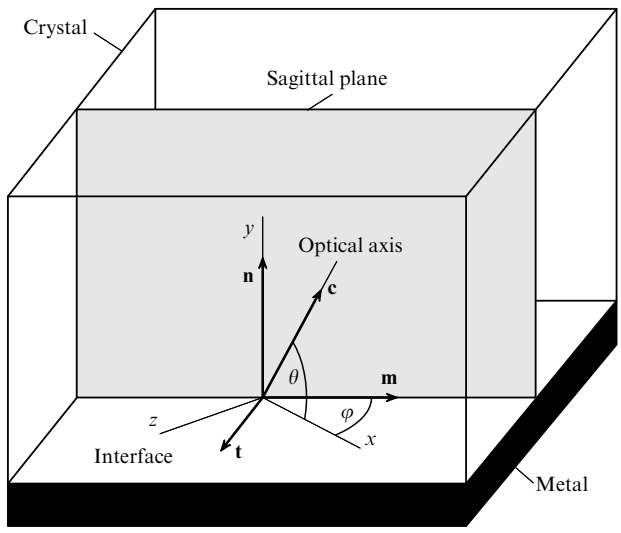

Figure 1. Wave geometry of plasmon-polariton propagation.

Fig. 1) can be represented as

$$\begin{pmatrix}\mathbf{H}(\mathbf{r},t)\\ \mathbf{E}(\mathbf{r},t)\end{pmatrix}=\begin{pmatrix}\mathbf{H}(y)\\ \mathbf{E}(y)\end{pmatrix}\exp\left[\mathrm{i}k(\mathbf{rm}-vt)\right],$$
$$\begin{pmatrix}\mathbf{H}(y)\\ \mathbf{E}(y)\end{pmatrix}=\begin{cases}\left[C_{\mathrm{o}}\begin{pmatrix}\mathbf{H}_{\mathrm{o}}\\ \mathbf{E}_{\mathrm{o}}\end{pmatrix}\exp\left(-kq_{\mathrm{o}}y\right)\right.\\ \qquad\left.+C_{\mathrm{e}}\begin{pmatrix}\mathbf{H}_{\mathrm{e}}\\ \mathbf{E}_{\mathrm{e}}\end{pmatrix}\exp\left[k(-q_{\mathrm{e}}+\mathrm{i}p_{\mathrm{e}})y\right]\right]_{y\geqslant 0},\\ \left[C^{\mathrm{TM}}\begin{pmatrix}\mathbf{H}^{\mathrm{TM}}\\ \mathbf{E}^{\mathrm{TM}}\end{pmatrix}+C^{\mathrm{TE}}\begin{pmatrix}\mathbf{H}^{\mathrm{TE}}\\ \mathbf{E}^{\mathrm{TE}}\end{pmatrix}\right]\exp\left(kq_{\mathrm{m}}y\right)_{y\leqslant 0}.\end{cases}\tag{2}$$

Here, $\mathbf{r}=(x,y,z)$ is the radius vector of the observation point and k is the length of the common component of the wave vectors of all partial waves along the propagation direction $\mathbf{m}$. The quantity k sets the tracing phase velocity $v=\omega/k$ of the plasmon-polariton along the interface and its wavelength $\lambda=2\pi/k$. For a given frequency ω, it is these quantities that are the unknown characteristics of the plasmon-polariton. However, the quantitates that are usually searched for in such problems are not k or λ, but the refractive index $n=c/v$, where c is the speed of light in a vacuum. Consequently, it is convenient to replace the wave vectors of partial waves $\mathbf{k}_\alpha$ in the sagittal plane $(\mathbf{m},\mathbf{n})$ with dimensionless refraction vectors $\mathbf{k}^0_\alpha=(c/\omega)\mathbf{k}_\alpha$ $(\alpha=\mathrm{o},\mathrm{e},\mathrm{m})$:

$$\begin{aligned}\mathbf{k}^0_{\mathrm{o}}&=(\mathbf{m}+\mathrm{i}q_{\mathrm{o}}\mathbf{n})n\,,\\ \mathbf{k}^0_{\mathrm{e}}&=\left\{\mathbf{m}+(\mathrm{i}q_{\mathrm{e}}+p_{\mathrm{e}})\mathbf{n}\right\}n\,,\\ \mathbf{k}^0_{\mathrm{m}}&=(\mathbf{m}-\mathrm{i}q_{\mathrm{m}}\mathbf{n})n\,.\end{aligned}\tag{3}$$

Partial waves in superposition (2) must individually satisfy Maxwell's equations. Therefore, all the parameters of each of the four waves in (2), except for the scalar amplitudes C_{o}, C_{e}, C^{TM}, and C^{TE}, are found by substituting them into the corresponding system of Maxwell's equations for a crystal or metal. As a result, the structure of expressions (3) is obtained, from which it follows that, out of all partial waves, the extraordinary mode alone has a nonzero real part of the y component of the wave vector $(\mathrm{Re}\,\mathbf{k}_{\mathrm{e}}\mathbf{n}=kp_{\mathrm{e}})$. Moreover, the parameter p_{e} does not depend on the refraction index n:

$$p_{\mathrm{e}}=\frac{c_{\mathbf{m}}c_{\mathbf{n}}(\varepsilon_{\mathrm{o}}-\varepsilon_{\mathrm{e}})}{\varepsilon_{\mathrm{o}}A}\,.\tag{4}$$

All imaginary parts of vectors $\mathbf{k}^0_\alpha$ (3) are characterized by localization parameters

$$\begin{aligned}&q_{\mathrm{o}}=\sqrt{1-s}\,,\qquad q_{\mathrm{e}}=\sqrt{\left(\frac{B}{A}-s\right)\frac{\varepsilon_{\mathrm{e}}}{\varepsilon_{\mathrm{o}}A}}\,,\\ &q_{\mathrm{m}}=\sqrt{1-\frac{\varepsilon_{\mathrm{m}}}{\varepsilon_{\mathrm{o}}}s}\,,\qquad s\equiv\frac{\varepsilon_{\mathrm{o}}}{n^2}\,,\end{aligned}\tag{5}$$

depending on the index n, instead of which a more convenient parameter s is introduced in (5). In Eqns (4) and (5), A and B are functions of the direction of the optical axis $\mathbf{c}$:

$$A=1+c^2_{\mathbf{n}}\varDelta_{\mathrm{o}}\,,\qquad B=1-c^2_{\mathbf{t}}\varDelta_{\mathrm{e}}\,,\tag{6}$$

where the projections $c_{\mathbf{n}}$ and $c_{\mathbf{t}}$ are determined by Eqn (1), and the parameters $\varDelta_{\mathrm{o,e}}$ are determined by the formula

$$\varDelta_\alpha=\frac{\varepsilon_{\mathrm{e}}-\varepsilon_{\mathrm{o}}}{\varepsilon_\alpha}\,,\qquad \alpha=\mathrm{o},\mathrm{e}\,.\tag{7}$$

Optically 'positive' $(\varepsilon_{\mathrm{e}}>\varepsilon_{\mathrm{o}})$ and 'negative' $(\varepsilon_{\mathrm{e}}<\varepsilon_{\mathrm{o}})$ crystals are usually distinguished. In crystals of the former type, $\varDelta_\alpha>0$, and, as the argument grows, the function $A(c^2_{\mathbf{n}})$ increases, and $B(c^2_{\mathbf{t}})$ decreases. In crystals of the latter type, $\varDelta_\alpha<0$ and functions (6) behave in the opposite way.

In Eqns (2), the polarization vectors of the ordinary and extraordinary partial polariton waves in the crystal are also found directly from Maxwell's equations:

$$\begin{aligned}\begin{pmatrix}\mathbf{H}_{\mathrm{o}}\\ \mathbf{E}_{\mathrm{o}}\end{pmatrix}&=N_{\mathrm{o}}\begin{pmatrix}\mathbf{k}^0_{\mathrm{o}}\times(\mathbf{k}^0_{\mathrm{o}}\times\mathbf{c})\\ \mathbf{k}^0_{\mathrm{o}}\times\mathbf{c}\end{pmatrix},\\ \begin{pmatrix}\mathbf{H}_{\mathrm{e}}\\ \mathbf{E}_{\mathrm{e}}\end{pmatrix}&=N_{\mathrm{e}}\begin{pmatrix}\mathbf{k}^0_{\mathrm{e}}\times\mathbf{c}\\ \mathbf{c}-\mathbf{k}^0_{\mathrm{e}}(\mathbf{k}^0_{\mathrm{e}}\,\mathbf{c})/\varepsilon_{\mathrm{o}}\end{pmatrix},\end{aligned}\tag{8}$$

where $N_{\mathrm{o,e}}$ are normalization constants. The vector amplitudes of the plasmon in a metal are found similarly:

$$\begin{aligned}\begin{pmatrix}\mathbf{H}^{\mathrm{TM}}\\ \mathbf{E}^{\mathrm{TM}}\end{pmatrix}&=\begin{pmatrix}\mathbf{t}\\ \mathbf{t}\times\mathbf{k}^0_{\mathrm{m}}/\varepsilon_{\mathrm{m}}\end{pmatrix},\\ \begin{pmatrix}\mathbf{H}^{\mathrm{TE}}\\ \mathbf{E}^{\mathrm{TE}}\end{pmatrix}&=\begin{pmatrix}-\mathbf{t}\times\mathbf{k}^0_{\mathrm{m}}\\ \mathbf{t}\end{pmatrix}.\end{aligned}\tag{9}$$

Equations (2) show that the TM and TE components of the plasmon are characterized by the same localization (the same parameter q_{m}). The conventional separation of a plasmon in an isotropic metal into two components is conditional and only done for convenience. Polarizations (9) are oriented in such a way that the pair $\mathbf{H}^{\mathrm{TM}}\parallel\mathbf{E}^{\mathrm{TE}}$ is orthogonal to the sagittal plane $(\mathbf{m},\mathbf{n})$, while the pair $\mathbf{E}^{\mathrm{TM}}\parallel\mathbf{H}^{\mathrm{TE}}$ is parallel to this plane.

3. Dispersion equation for an arbitrary interface orientation

The boundary conditions, which are standard for the problem under consideration [1], are reduced to the requirement of continuity of the tangential components of the magnetic and electric fields at the interface between the media, $y=0$. These conditions determine the scalar amplitudes C_α in Eqns (2), leading to a system of homogeneous equations

$$\begin{pmatrix}\mathrm{i}q_{\mathrm{o}}a & bc_{\mathbf{t}} & 0 & \mathrm{i}q_{\mathrm{m}}\\ sc_{\mathbf{t}} & bc_{\mathbf{m}}-c_{\mathbf{n}} & 1 & 0\\ -\mathrm{i}q_{\mathrm{o}}sc_{\mathbf{t}} & q^2_{\mathrm{o}}c_{\mathbf{m}}+bc_{\mathbf{n}} & \mathrm{i}q_{\mathrm{m}}\varepsilon_{\mathrm{o}}/\varepsilon_{\mathrm{m}} & 0\\ a & c_{\mathbf{t}} & 0 & -1\end{pmatrix}\begin{pmatrix}C_{\mathrm{o}}\\ C_{\mathrm{e}}\\ C^{\mathrm{TM}}\\ C^{\mathrm{TE}}\end{pmatrix}=0\,,\tag{10}$$

where, to simplify the matrix, the scalar amplitudes from (2) are renormalized,

$$C_{\mathrm{o}}\to\frac{C_{\mathrm{o}}}{n^2}\,,\quad C_{\mathrm{e}}\to\frac{C_{\mathrm{e}}}{n}\,,\quad C^{\mathrm{TM}}\to C^{\mathrm{TM}}\,,\quad C^{\mathrm{TE}}\to\frac{C^{\mathrm{TE}}}{n}\,,\tag{11}$$

and the following notations are introduced:

$$a=c_{\mathbf{n}}-\mathrm{i}q_{\mathrm{o}}c_{\mathbf{m}}\,,\qquad b=p_{\mathrm{e}}+\mathrm{i}q_{\mathrm{e}}\,.\tag{12}$$

The condition for the existence of nontrivial solutions of the homogeneous system (10) for the amplitude coefficients C_α, as usual, reduces to the requirement that the determinant of the 4×4 matrix in (10) vanish, which yields the complex

dispersion equation

$$D \equiv \mathrm{i}a\big[\varepsilon_{\mathrm{m}}(q_{\mathrm{o}}^2 c_{\mathbf{m}} + b c_{\mathbf{n}}) + \mathrm{i}\varepsilon_{\mathrm{o}} q_{\mathrm{m}}(c_{\mathbf{n}} - b c_{\mathbf{m}})\big] + \mathrm{i}\varepsilon_{\mathrm{o}} c_{\mathbf{t}}(b + \mathrm{i}q_{\mathrm{m}})(1 - q_{\mathrm{o}} q_{\mathrm{m}}) = 0\,. \tag{13}$$

As noted in the introduction, complex dispersion equation (13), decomposing into two equations, should be equivalent to one real equation. We now prove this assertion in an explicit way. The real and imaginary parts in determinant D (13) are singled out and transformed using the identities

$$c_{\mathbf{n}} - p_{\mathrm{e}} c_{\mathbf{m}} = \frac{\varepsilon_{\mathrm{e}}}{\varepsilon_{\mathrm{o}}}\frac{c_{\mathbf{n}}}{A}(1 - \Delta_{\mathrm{e}} c_{\mathbf{t}}^2)\,, \qquad q_{\mathrm{o}}^2 c_{\mathbf{m}} + p_{\mathrm{e}} c_{\mathbf{n}} = c_{\mathbf{m}}\left(\frac{\varepsilon_{\mathrm{o}} A}{\varepsilon_{\mathrm{e}}}\, q_{\mathrm{e}}^2 + \frac{\Delta_{\mathrm{e}} c_{\mathbf{t}}^2}{A}\right), \tag{14}$$

$$A q_{\mathrm{o}}^2 - \frac{\varepsilon_{\mathrm{o}}}{\varepsilon_{\mathrm{e}}}(A q_{\mathrm{e}})^2 = c_{\mathbf{n}}^2 \Delta_{\mathrm{o}} + c_{\mathbf{t}}^2 \Delta_{\mathrm{e}}\,, \qquad s = 1 - q_{\mathrm{o}}^2 = \frac{\varepsilon_{\mathrm{o}}(q_{\mathrm{o}} + q_{\mathrm{m}})(1 - q_{\mathrm{o}} q_{\mathrm{m}})}{\varepsilon_{\mathrm{m}} q_{\mathrm{o}} + \varepsilon_{\mathrm{o}} q_{\mathrm{m}}}\,. \tag{15}$$

As a result, we obtain

$$\operatorname{Re} D = c_{\mathbf{m}}^2 q_{\mathrm{o}} G_1 - c_{\mathbf{n}}^2 G_2 - c_{\mathbf{t}}^2 (q_{\mathrm{e}} + q_{\mathrm{m}}) G_3\,, \qquad \operatorname{Im} D = c_{\mathbf{m}} c_{\mathbf{n}}\left(G_1 + q_{\mathrm{o}} G_2 - \frac{\Delta_{\mathrm{o}}}{A}\, G_3\right), \tag{16}$$

where

$$G_1 = \frac{\varepsilon_{\mathrm{o}}}{\varepsilon_{\mathrm{e}}}\, q_{\mathrm{e}}(\varepsilon_{\mathrm{m}} A q_{\mathrm{e}} + \varepsilon_{\mathrm{e}} q_{\mathrm{m}}) + \frac{\varepsilon_{\mathrm{m}}}{A}\, c_{\mathbf{t}}^2 \Delta_{\mathrm{e}} = \varepsilon_{\mathrm{m}}\left(q_{\mathrm{o}}^2 - 1 + \frac{1}{A}\right) + \varepsilon_{\mathrm{o}} q_{\mathrm{e}} q_{\mathrm{m}} \equiv G_1'\,,$$
$$G_2 = \frac{c_{\mathbf{n}}}{A}\left[\varepsilon_{\mathrm{m}} A q_{\mathrm{e}} + \varepsilon_{\mathrm{e}} q_{\mathrm{m}}(1 - c_{\mathbf{t}}^2 \Delta_{\mathrm{e}})\right], \quad G_3 = \varepsilon_{\mathrm{o}}(1 - q_{\mathrm{o}} q_{\mathrm{m}})\,. \tag{17}$$

Here, G_1 and G_1' are alternative forms of the same relation, both of which are used below. Substituting (17) into the formula for $\operatorname{Im} D$ in Eqn (16), we easily obtain

$$\operatorname{Im} D = \frac{c_{\mathbf{m}} c_{\mathbf{n}}}{A}\, F(s)\,, \tag{18}$$

where $F(s)$ is a real function:

$$F(s) = \left(q_{\mathrm{o}} + \frac{\varepsilon_{\mathrm{o}}}{\varepsilon_{\mathrm{e}}}\, A q_{\mathrm{e}}\right)(\varepsilon_{\mathrm{m}} A q_{\mathrm{e}} + \varepsilon_{\mathrm{e}} q_{\mathrm{m}}) - c_{\mathbf{t}}^2 \Delta_{\mathrm{e}}(\varepsilon_{\mathrm{e}} - \varepsilon_{\mathrm{m}})\,. \tag{19}$$

A similar procedure with the substitution of (17) into the formula for $\operatorname{Re} D$ in (16) yields the result after more cumbersome calculations. In this case, it is convenient to use both forms of identically equal expressions $G_1 \equiv G_1'$:

$$\operatorname{Re} D = q_{\mathrm{o}} G_1 - c_{\mathbf{n}}^2(q_{\mathrm{o}} G_1 + G_2) - c_{\mathbf{t}}^2\left[q_{\mathrm{o}} G_1' + (q_{\mathrm{e}} + q_{\mathrm{m}}) G_3\right] = \frac{q_{\mathrm{e}} - q_{\mathrm{o}}}{\Delta_{\mathrm{o}}}\, F(s)\,, \tag{20}$$

where $F(s)$ is the same function (19). Thus, the complex determinant D (13) is indeed proportional to the same real function:

$$D = \left(\frac{\varepsilon_{\mathrm{o}}(q_{\mathrm{e}} - q_{\mathrm{o}})}{\varepsilon_{\mathrm{e}} - \varepsilon_{\mathrm{o}}} + \mathrm{i}\,\frac{c_{\mathbf{m}} c_{\mathbf{n}}}{A}\right) F(s)\,. \tag{21}$$

Thus, we have arrived at a real universal dispersion equation, which is valid for an arbitrary orientation of the crystal:

$$(\varepsilon_{\mathrm{e}} q_{\mathrm{o}} + \varepsilon_{\mathrm{o}} A q_{\mathrm{e}})(\varepsilon_{\mathrm{m}} A q_{\mathrm{e}} + \varepsilon_{\mathrm{e}} q_{\mathrm{m}}) = c_{\mathbf{t}}^2(\varepsilon_{\mathrm{e}} - \varepsilon_{\mathrm{o}})(\varepsilon_{\mathrm{e}} - \varepsilon_{\mathrm{m}})\,. \tag{22}$$

At first glance, the complex factor in brackets in (21) could provide additional dispersion branches at $q_{\mathrm{o}} = q_{\mathrm{e}}$, when the optical axis $\mathbf{c}$ lies in one of the coordinate planes: $c_{\mathbf{m}} = 0$ or $c_{\mathbf{n}} = 0$. However, analysis shows that this hypothetical possibility is not realized.

Under condition (22), the homogeneous system of equations (10) defines the following relations between scalar amplitudes:

$$\frac{C_{\mathrm{o}}}{C^{\mathrm{TM}}} = \frac{-b - \mathrm{i}q_{\mathrm{m}}}{Z}\, c_{\mathbf{t}}\,, \qquad \frac{C_{\mathrm{e}}}{C^{\mathrm{TM}}} = \frac{\mathrm{i}(q_{\mathrm{o}} + q_{\mathrm{m}})a}{Z}\,,$$
$$\frac{C^{\mathrm{TE}}}{C^{\mathrm{TM}}} = \frac{(-b + \mathrm{i}q_{\mathrm{o}})a}{Z}\, c_{\mathbf{t}}\,, \qquad Z = c_{\mathbf{t}}^2(b + \mathrm{i}q_{\mathrm{m}})s + \mathrm{i}(q_{\mathrm{o}} + q_{\mathrm{m}})(-b c_{\mathbf{m}} + c_{\mathbf{n}})a\,. \tag{23}$$

Result (22) is a generalization of the well-known Dyakonov equation [7, 28, 29] for the special case of an interface chosen to be parallel to the optical axis: $c_{\mathbf{n}} = 0$. We now show that Eqn (22) at $c_{\mathbf{n}} = 0$ $(A = 1)$ actually yields this equation. Substitution of the identity $c_{\mathbf{t}}^2(\varepsilon_{\mathrm{e}} - \varepsilon_{\mathrm{o}}) = q_{\mathrm{o}}^2 \varepsilon_{\mathrm{e}} - q_{\mathrm{e}}^2 \varepsilon_{\mathrm{o}}$ into (22) (see (15) for $A = 1$) gives the equation

$$(\varepsilon_{\mathrm{m}} q_{\mathrm{o}} + \varepsilon_{\mathrm{o}} q_{\mathrm{e}})(q_{\mathrm{m}} + q_{\mathrm{e}}) = q_{\mathrm{o}}(q_{\mathrm{m}} - q_{\mathrm{o}})(\varepsilon_{\mathrm{m}} - \varepsilon_{\mathrm{e}})\,, \tag{24}$$

which looks even more compact than the classic version of the Dyakonov equation. Multiplication of (24) by $(q_{\mathrm{m}} + q_{\mathrm{o}})$ leads to the Dyakonov equation, yielding the well-known form [7], which in our terms has the form

$$(\varepsilon_{\mathrm{m}} q_{\mathrm{o}} + \varepsilon_{\mathrm{o}} q_{\mathrm{e}})(q_{\mathrm{m}} + q_{\mathrm{e}})(q_{\mathrm{m}} + q_{\mathrm{o}}) = \frac{q_{\mathrm{o}}(\varepsilon_{\mathrm{e}} - \varepsilon_{\mathrm{m}})(\varepsilon_{\mathrm{m}} - \varepsilon_{\mathrm{o}})}{n^2}\,. \tag{25}$$

Here, the identity

$$q_{\mathrm{m}}^2 - q_{\mathrm{o}}^2 = \frac{\varepsilon_{\mathrm{o}} - \varepsilon_{\mathrm{m}}}{n^2} \tag{26}$$

was taken into account.

Equation (25) was originally obtained in [7] to describe a polariton at the interface between two dielectrics, a uniaxial crystal and an isotropic medium, when all three permittivity values, ε_{o}, ε_{e}, and ε_{m}, are positive. According to [7], the solution of Eqn (25) can only be realized in positive crystals, and only if the value ε_{m} lies between ε_{o} and ε_{e}:

$$0 < \varepsilon_{\mathrm{o}} < \varepsilon_{\mathrm{m}} < \varepsilon_{\mathrm{e}}\,. \tag{27}$$

It was shown later [8, 9] that the necessary condition for the existence of a polariton (27) remains valid for an arbitrary orientation of the interface. According to [7–9], the geometric dimensions of the region of existence in terms of the angles (θ, φ) are not small only for highly anisotropic crystals. In this case, criterion (27) precludes the propagation of a polariton along the interface of two isotropic dielectrics.

We do not compare here dispersion equation (22) with the corresponding equations presented in [8, 9], which remained complex (like (13)) and were further analyzed using numerical [8] or approximate [9] approaches. Presented below is an analytical description of the plasmon polariton. It should also

be noted that, in the case of the metallic isotropic medium under consideration ($\varepsilon_{\rm m} < 0$), the solutions of Eqn (22) radically differ from those obtained in [7–9]. In this case, condition (27) apparently fails. In subsequent sections, we show that the plasmon-polariton exists in crystals of both signs in a wide range of interface orientations.

4. Exact solution of the dispersion equation for a special geometry

We now consider the orientation of the plasmon-polariton propagation that corresponds to the choice of the sagittal plane parallel to the optical axis: $\varphi = 0$, i.e., $c_{\mathbf{t}} = 0$ when the problem under study has an exact solution. In this case, equation (22) decomposes into two independent dispersion equations. The first of them is

$$\varepsilon_{\rm e} q_{\rm o} + \varepsilon_{\rm o} A q_{\rm e} = 0\,; \tag{28}$$

in the case under consideration, the positive permittivity values of the crystal $\varepsilon_{\rm o}$ and $\varepsilon_{\rm e}$ can only be satisfied if the parameters $q_{\rm o} = q_{\rm e} = 0$ simultaneously vanish. Equations (5) and (6) then show that equalities $A = B = 1$ and $c_{\mathbf{t}} = c_{\mathbf{n}} = 0$ should be fulfilled, which corresponds to the propagation of a bulk polariton along the optical axis ($\mathbf{m} = \mathbf{c}$) lying in the interface plane. We now show that such a solution is not possible.

An important remark should be made here. In formulas (8) for the polarization vectors of partial waves in crystals, normalization constants $N_{\rm o,e}$ are introduced, which have not played any significant role so far. No attention whatsoever need be given them in analyzing almost any wave situation, but not for this singular case. It can be easily seen that, without normalization in this case, all vector amplitudes in (8) vanish, as do most of the matrix elements in system (10). However, after normalization ($|\mathbf{E}_{\rm o,e}| = 1$) in (8) with $c_{\mathbf{n}} = c_{\mathbf{t}} = 0$ (i.e., $\mathbf{c} = \mathbf{m}$) and $q_{\rm o}, q_{\rm e} \to 0$, $n^2 \to \varepsilon_{\rm o}$, we obtain, taking into account (3),

$$\begin{pmatrix} \mathbf{H}_{\rm o} \\ \mathbf{E}_{\rm o} \end{pmatrix} = N_{\rm o} \begin{pmatrix} \mathbf{k}_{\rm o}^0 \times (\mathbf{k}_{\rm o}^0 \times \mathbf{m}) \\ \mathbf{k}_{\rm o}^0 \times \mathbf{m} \end{pmatrix} = \begin{pmatrix} -n\mathbf{n} \\ \mathbf{t} \end{pmatrix}, \qquad \begin{pmatrix} \mathbf{H}_{\rm e} \\ \mathbf{E}_{\rm e} \end{pmatrix} = N_{\rm e} \begin{pmatrix} \mathbf{k}_{\rm e}^0 \times \mathbf{m} \\ \mathbf{m} - \mathbf{k}_{\rm e}^0 (\mathbf{k}_{\rm e}^0 \mathbf{m})/\varepsilon_{\rm o} \end{pmatrix} = \begin{pmatrix} n\mathbf{t} \\ \mathbf{n} \end{pmatrix}. \tag{29}$$

Now, the general complex equation (10) after simplifications takes the form

$$\begin{pmatrix} 0 & 0 & 0 & 1 \\ 0 & n & 1 & 0 \\ 0 & 0 & 1 & 0 \\ 1 & 0 & 0 & -1 \end{pmatrix} \begin{pmatrix} C_{\rm o} \\ C_{\rm e} \\ C^{\rm TM} \\ C^{\rm TE} \end{pmatrix} = 0\,. \tag{30}$$

It can be easily seen that the determinant of the matrix on the left side of system (30) is nonzero:

$$D_0 = -n \neq 0\,, \tag{31}$$

thus indicating the absence of nontrivial solutions to system (30) and hence a prohibition on the existence of the proposed plasmon-polariton.

Thus, for $c_{\mathbf{t}} = 0$, dispersion equation (22) takes the simple form

$$\varepsilon_{\rm m} A q_{\rm e} + \varepsilon_{\rm e} q_{\rm m} = 0\,. \tag{32}$$

We have already derived this equation earlier [30] by direct analysis of the problem for a given special orientation.

Substituting the functions $q_{\rm e}(s)$ and $q_{\rm m}(s)$ (5) at $B = 1$ into (32), we find the solution

$$s = \frac{1 - \varepsilon_{\rm o}\varepsilon_{\rm e}/\varepsilon_{\rm m}^2}{A - \varepsilon_{\rm e}/\varepsilon_{\rm m}}\,, \tag{33}$$

which determines via Eqns (5) all the wave parameters of the plasmon-polariton:

$$q_{\rm o} = \sqrt{1 - \frac{1 - \varepsilon_{\rm o}\varepsilon_{\rm e}/\varepsilon_{\rm m}^2}{A - \varepsilon_{\rm e}/\varepsilon_{\rm m}}}\,, \tag{34}$$

$$q_{\rm e} = \frac{1}{A}\sqrt{\frac{\varepsilon_{\rm e}}{\varepsilon_{\rm o}}\left(\frac{1 - A\varepsilon_{\rm o}/\varepsilon_{\rm m}}{1 - A\varepsilon_{\rm m}/\varepsilon_{\rm e}}\right)}\,, \tag{35}$$

$$q_{\rm m} = \sqrt{\frac{A - \varepsilon_{\rm m}/\varepsilon_{\rm o}}{A - \varepsilon_{\rm e}/\varepsilon_{\rm m}}}\,. \tag{36}$$

Wave parameters (33)–(36) are functions of the angle of inclination θ of the optical axis $\mathbf{c}$ to the interface plane, since the quantity A (6) in these formulas depends on $c_{\mathbf{n}}^2 = \sin^2\theta$ (Fig. 1 at $\varphi = 0$). It should be noted in passing that the absence of bulk solutions of Eqn (28) along the optical axis $\mathbf{c} \parallel \mathbf{m}$, which was proven above, does not apply to localized waves, which are described by formulas (33)–(36) at $\theta = 0$.

Figure 2 shows the dependences on θ of wave parameters (5) and (33)–(36) for two positive and two negative crystals in contact with gold at a wavelength in vacuum $\lambda_{\rm vac} = 2\pi c/\omega = 0.75$ μm, when $\varepsilon_{\rm m} = -20.148$ for gold [31]. The material parameters for $NaNO_3$ were taken from [22], and for the other three crystals, data reported in [32] were used. As can be seen from formulas (33)–(36) and Fig. 2, the dependences found for positive (a, b) and negative (c, d) crystals have a different behavior. In the former case, the functions $n(\theta)$ and $q_{\rm o}(\theta)$ increase with increasing θ, while the functions $q_{\rm e,m}(\theta)$ decrease; in the latter case, the opposite is true.

It should be noted, however, that the structure of the plasmon-polariton in this geometry is greatly simplified. According to (23), at $c_{\mathbf{t}} = 0$, we have $C_{\rm o} = C^{\rm TE} = 0$, so wave superposition (2) only contains two partial components: the e-wave in a crystal and the TM mode in a metal with the following amplitude ratio:

$$\frac{C^{\rm TM}}{C_{\rm e}} = -bc_{\mathbf{m}} + c_{\mathbf{n}}\,. \tag{37}$$

Taking into account the zero amplitude of the ordinary wave ($C_{\rm o} = 0$), curves $q_{\rm o}(\theta)$ are shown in Fig. 2 as dashed lines. Their presence in the figure is justified by the fact that, for any deviation of the sagittal plane from the orientation $c_{\mathbf{t}} = 0$, the existing superposition of e- and TM-waves ($C_{\rm e}, C^{\rm TM} \neq 0$) will have admixed o- and TE-waves with amplitudes $C_{\rm o}$ and $C^{\rm TE}$; the stronger the perturbation $c_{\mathbf{t}}$ in (23), the greater the amplitudes. In practice, this situation always occurs, if only because of the inevitable diffraction divergence of the beam.

Formally, the domain where solutions (33)–(36) exist is limited by the condition $s > 0$ and the requirement that the parameters q_α be real. If $\varepsilon_{\rm m} < 0$, the denominator in (33) is certainly greater than zero; therefore, the positivity of s is only violated for $\varepsilon_{\rm m}^2 \leqslant \varepsilon_{\rm o}\varepsilon_{\rm e}$. However, the region of small $|\varepsilon_{\rm m}|$ is of no practical interest due to the strong attenuation of the

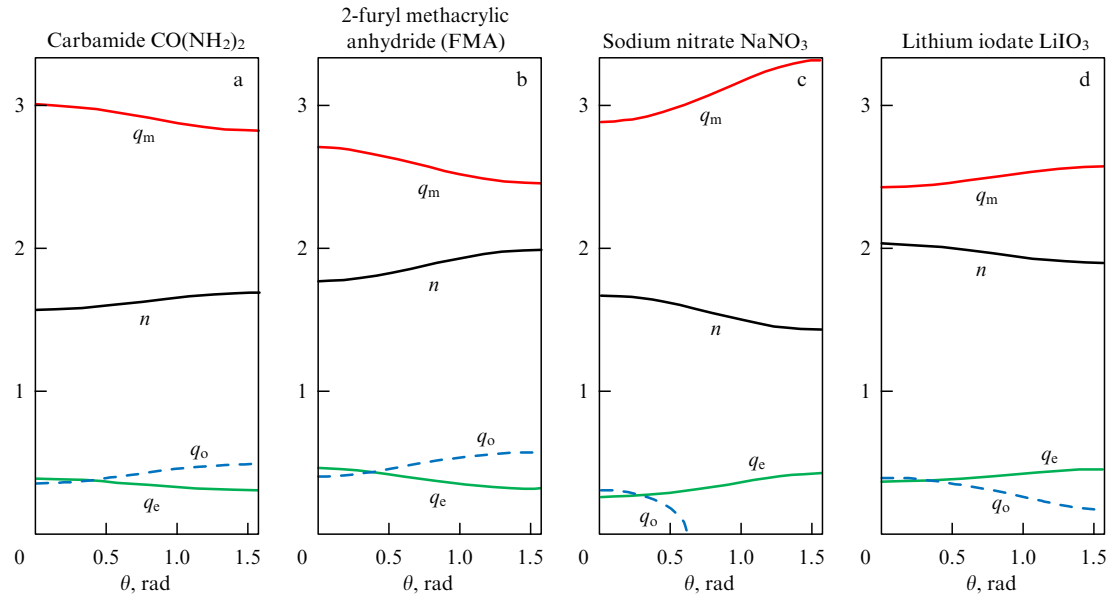

Figure 2. Dependences $n(\theta)$, $q_o(\theta)$, $q_e(\theta)$, and $q_m(\theta)$ for two positive (a, b) and two negative (c, d) crystals.

plasmon in the dissipating metal. For the plasmon-polariton path length to significantly exceed the wavelength, the value of $|\varepsilon_m|$ should be greatly increased, passing into the infrared region, which is rather characterized by the opposite relationship $\varepsilon_m^2 \gg \varepsilon_o\varepsilon_e$.

As can be seen from Eqns (35) and (36), the parameters $q_{e,m}$ are real and positive for any characteristics of media and orientations θ of the optical axis in the sagittal plane $\{\mathbf{m}, \mathbf{n}\}$. Therefore, they cannot limit the region where the plasmon-polariton under consideration exists. However, the reality of the parameter q_o (34) (taking into account the admixture of o- and TE-waves) is by no means guaranteed. The q_o parameter only remains real until the sign of the radical expression in (34) is changed:

$$\varepsilon_o\varepsilon_e(\varepsilon_o - \varepsilon_m) \geqslant c_{\mathbf{n}}^2\varepsilon_m^2(\varepsilon_o - \varepsilon_e)\,. \tag{38}$$

Condition (38) can only be violated for negative crystals ($\varepsilon_e < \varepsilon_o$). The critical inclination θ_c of the optical axis corresponding to $q_o = 0$ is determined by the condition

$$\sin^2\theta_c = \frac{\varepsilon_o\varepsilon_e}{\varepsilon_m^2}\,\frac{\varepsilon_o - \varepsilon_m}{\varepsilon_o - \varepsilon_e} \equiv (c_{\mathbf{n}}^2)_{\max} \leqslant 1\,. \tag{39}$$

In Figure 2c, the dashed curve of the $q_o(\theta)$ function for the $NaNO_3$ crystal shows the violation of criterion (38) at $\theta > \theta_c \approx 0.62$ rad. Of course, the limiting angle θ_c (39) does not necessarily exist: there is none in the $LiIO_3$ crystal (Fig. 2d). On the other hand, the presence of such limiting orientations is not uncommon. As the wavelength increases, the quantity $|\varepsilon_m|$ increases rapidly, and the angle θ_c (39) decreases accordingly. For example, with an increase in λ_{vac} from 0.75 to 1 μm for gold, we have [31] $\varepsilon_m = -41.849$ instead of -20.148, so the limiting angle also appears in the $LiIO_3$ crystal: $\theta_c = 0.82$ rad.

If $\theta = \theta_c$, the partial o-wave becomes a bulk wave, and at $\theta > \theta_c$ this bulk wave acquires a nonzero real component k_y and starts removing energy from the interface — the polariton becomes leaky, i.e., is characterized by a decrease in the tangential component of the energy flux as it propagates and, consequently, by a nondissipative limitation of the path length.

Thus, the region of orientations of the optical axis $\theta > \theta_c$ is the region of instability of the two-partial plasmon-polariton under study. In this region, for any perturbation in orientation that drives the optical axis out of the sagittal plane $c_{\mathbf{t}} = 0$, the surface polariton in the crystal transforms into a pseudo-surface one.

5. Approximate solution in the Dyakonov geometry by the iteration method

In this section, we consider the orientation $c_{\mathbf{n}} = 0$, which was studied in Dyakonov's theory of polaritons [7] (see Section 3). The same geometry was later analyzed in the theory of plasmon-polaritons, but primarily by numerical methods [28, 29]. Here, as before, our goal is to develop an analytical theory that expresses the wave characteristics of a plasmon-polariton as a function of material and geometrical parameters. It should be noted that Dyakonov [7] already proposed an approximate analytical solution of Eqn (25) for a polariton based on the assumption that the crystal anisotropy is small. The concept of the solution is based on the observation that under conditions (27) the quantities ε_o and ε_e being close to each other implies that the product $(\varepsilon_e - \varepsilon_m)(\varepsilon_m - \varepsilon_o)$ on the right side of equation (25) is small. The approximation used in [9] was based on similar considerations. In the case of a plasmon-polariton, when $|\varepsilon_m| \gg 1$ and $\varepsilon_m < 0$, this product is large rather than small, so we have to look for alternative approaches to the solution.

We consider the case of the optical axis of a crystal parallel to the interface plane $\{\mathbf{m}, \mathbf{t}\}$ (see Fig. 1), so that $\theta = 0$ and $A = 1$ (6). Dispersion equation (22) for the propagation geometry under consideration can be conveniently represented as

$$\frac{q_e}{\varepsilon_e} + \frac{q_m}{\varepsilon_m} = -\frac{c_{\mathbf{t}}^2\Delta_e}{\varepsilon_o q_e + \varepsilon_e q_o}\left(1 - \frac{\varepsilon_e}{\varepsilon_m}\right). \tag{40}$$

The dependence of wave parameters on orientation in Eqn (40) is now determined by the parameter $c_{\mathbf{t}}^2 = \sin^2\varphi$, both explicitly and implicitly, via the parameter q_{e} (5).

To remove radicals (5) from the left part of Eqn (40), we multiply this equation by the factor

$$\varepsilon_{\mathrm{o}}\varepsilon_{\mathrm{e}}\left(\frac{q_{\mathrm{e}}}{\varepsilon_{\mathrm{e}}} - \frac{q_{\mathrm{m}}}{\varepsilon_{\mathrm{m}}}\right) \neq 0\,. \tag{41}$$

As a result, the left part of the equation takes the form

$$\frac{\varepsilon_{\mathrm{o}}}{\varepsilon_{\mathrm{e}}}\,q_{\mathrm{e}}^2 - \frac{\varepsilon_{\mathrm{o}}\varepsilon_{\mathrm{e}}}{\varepsilon_{\mathrm{m}}^2}\,q_{\mathrm{m}}^2 \equiv q_{\mathrm{o}}^2 - \frac{\varepsilon_{\mathrm{o}}\varepsilon_{\mathrm{e}}}{\varepsilon_{\mathrm{m}}^2}\,q_{\mathrm{m}}^2 - c_{\mathbf{t}}^2\Delta_{\mathrm{e}}$$
$$\equiv 1 - \frac{\varepsilon_{\mathrm{o}}\varepsilon_{\mathrm{e}}}{\varepsilon_{\mathrm{m}}^2} - s\left(1 - \frac{\varepsilon_{\mathrm{e}}}{\varepsilon_{\mathrm{m}}}\right) - c_{\mathbf{t}}^2\Delta_{\mathrm{e}}\,, \tag{42}$$

where relations (5) and identity (26) at $A = 1$ are taken into account. Moving the term $c_{\mathbf{t}}^2\Delta_{\mathrm{e}}$ in Eqn (42) from the left to the right part of the equation obtained, after minor transformations, we derive a new form of the exact dispersion equation:

$$s - s^{(0)} = c_{\mathbf{t}}^2\Delta_{\mathrm{e}}\eta\,, \tag{43}$$

where

$$s^{(0)} = \frac{1 - \varepsilon_{\mathrm{o}}\varepsilon_{\mathrm{e}}/\varepsilon_{\mathrm{m}}^2}{1 - \varepsilon_{\mathrm{e}}/\varepsilon_{\mathrm{m}}}\,, \tag{44}$$

$$\eta = \frac{\varepsilon_{\mathrm{e}}}{\varepsilon_{\mathrm{e}} - \varepsilon_{\mathrm{m}}} - \frac{\kappa_{\mathrm{o}} - 1}{\kappa_{\mathrm{o}} + \kappa_{\mathrm{e}}}\,, \tag{45}$$

$$\kappa_{\mathrm{o}} = -\frac{q_{\mathrm{o}}\varepsilon_{\mathrm{m}}}{q_{\mathrm{m}}\varepsilon_{\mathrm{o}}}\,, \qquad \kappa_{\mathrm{e}} = -\frac{q_{\mathrm{e}}\varepsilon_{\mathrm{m}}}{q_{\mathrm{m}}\varepsilon_{\mathrm{e}}}\,. \tag{46}$$

Resulting exact equation (43) has a significant advantage over (22) and (40): it is well prepared for the forthcoming approximate calculations. As shown below, for many crystals, the right side in Eqn (43) is convincingly small compared to $s^{(0)} \sim 1$ for almost any orientation φ of the optical axis $\mathbf{c}$ in the interface plane. This provides us with an analytical description of the parameters and conditions for the existence of a plasmon-polariton with quite acceptable accuracy.

In the zeroth order, the right side of (43) is assumed to be equal to zero, so in this approximation the solution is given by formula (44), which coincides with (33) at $A = 1$. However, it should be remembered that exact formula (33) was obtained for the case $c_{\mathbf{t}} = 0$, $c_{\mathbf{n}} \neq 0$, and $B = 1$ and depended on the inclination θ of the optical axis $\mathbf{c}$ in the sagittal plane (see Fig. 1), while Eqn (44) was derived for $c_{\mathbf{n}} = 0$, $c_{\mathbf{t}} \neq 0$, and $A = 1$ as the zeroth-order solution, and in this approximation does not depend on orientation (azimuth φ). However, at $\varphi = 0$, this solution is also an exact solution. Definitely, here, as in Eqn (33), it is assumed that $\varepsilon_{\mathrm{m}}^2 > \varepsilon_{\mathrm{o}}\varepsilon_{\mathrm{e}}$.

In the zeroth approximation under consideration, by combining (44) with relations (5), we obtain the localization parameters $q_{\mathrm{o}}^{(0)}$, $q_{\mathrm{e}}^{(0)}$, and $q_{\mathrm{m}}^{(0)}$. The first and the third of these parameters do not depend on orientation $\mathbf{c}$,

$$q_{\mathrm{o}}^{(0)} = \sqrt{\frac{1 - \varepsilon_{\mathrm{o}}/\varepsilon_{\mathrm{m}}}{1 - \varepsilon_{\mathrm{m}}/\varepsilon_{\mathrm{e}}}}\,, \qquad q_{\mathrm{m}}^{(0)} = \sqrt{\frac{1 - \varepsilon_{\mathrm{m}}/\varepsilon_{\mathrm{o}}}{1 - \varepsilon_{\mathrm{e}}/\varepsilon_{\mathrm{m}}}} = q_{\mathrm{o}}^{(0)}\,\frac{-\varepsilon_{\mathrm{m}}}{\sqrt{\varepsilon_{\mathrm{o}}\varepsilon_{\mathrm{e}}}}\,, \tag{47}$$

since their anisotropy, according to (5), is fully determined by the parameter $s^{(0)}$. In contrast to these two parameters, the parameter $q_{\mathrm{e}}^{(0)}$ contains an additional source of anisotropy (via B) and is therefore fairly sensitive to variations in $c_{\mathbf{t}}$ already in the zeroth approximation:

$$q_{\mathrm{e}}^{(0)} = \sqrt{\frac{\varepsilon_{\mathrm{e}}}{\varepsilon_{\mathrm{o}}}\left(\frac{1 - \varepsilon_{\mathrm{o}}/\varepsilon_{\mathrm{m}}}{1 - \varepsilon_{\mathrm{m}}/\varepsilon_{\mathrm{e}}} - \Delta_{\mathrm{e}}c_{\mathbf{t}}^2\right)}\,. \tag{48}$$

As $c_{\mathbf{t}}$ grows, this parameter increases for negative crystals, decreases for positive crystals, and, in principle, can vanish at a certain value of $c_{\mathbf{t}}$.

The next approximation 'incorporates' the right-hand side of Eqn (43) with the parameters $q_{\mathrm{o}}^{(0)}$, $q_{\mathrm{e}}^{(0)}$, and $q_{\mathrm{m}}^{(0)}$ (47), (48) calculated in the zeroth approximation. As a result, we obtain

$$\kappa_{\mathrm{o}}^{(0)} = \sqrt{\frac{\varepsilon_{\mathrm{e}}}{\varepsilon_{\mathrm{o}}}}\,, \qquad \kappa_{\mathrm{e}}^{(0)} = \sqrt{\frac{B - s^{(0)}}{1 - s^{(0)}}} = \sqrt{1 - \frac{c_{\mathbf{t}}^2\Delta_{\mathrm{e}}}{(q_{\mathrm{o}}^{(0)})^2}}\,, \tag{49}$$

where the parameter B is defined in (6) and only depends on the azimuth φ, since, in the case under consideration, $\theta = 0$ (see Fig. 1): $c_{\mathbf{t}} = \sin\varphi$. Formulas (49) are derived from (5), (44) and the relationship between $q_{\mathrm{m}}^{(0)}$ and $q_{\mathrm{o}}^{(0)}$ in (47). Combining formulas (49) and (45), we obtain

$$\eta^{(0)} = \frac{\varepsilon_{\mathrm{e}}}{\varepsilon_{\mathrm{e}} - \varepsilon_{\mathrm{m}}} - \frac{\sqrt{\varepsilon_{\mathrm{e}}/\varepsilon_{\mathrm{o}}} - 1}{\sqrt{\varepsilon_{\mathrm{e}}/\varepsilon_{\mathrm{o}}} + \kappa_{\mathrm{e}}^{(0)}}\,. \tag{50}$$

Next, we substitute the first-order approximation into (43),

$$s \approx s^{(1)} = s^{(0)} + \delta s^{(1)}\,, \tag{51}$$

and, taking into account (50), we find

$$\delta s^{(1)} = c_{\mathbf{t}}^2\eta^{(0)}\Delta_{\mathrm{e}} = c_{\mathbf{t}}^2\left(\frac{\varepsilon_{\mathrm{e}} - \varepsilon_{\mathrm{o}}}{\varepsilon_{\mathrm{e}} - \varepsilon_{\mathrm{m}}} - \frac{(n_{\mathrm{e}} - n_{\mathrm{o}})^2(n_{\mathrm{e}} + n_{\mathrm{o}})}{\varepsilon_{\mathrm{e}}(n_{\mathrm{e}} + n_{\mathrm{o}}\kappa_{\mathrm{e}}^{(0)})}\right)\,, \tag{52}$$

where $n_{\mathrm{o}} = \sqrt{\varepsilon_{\mathrm{o}}}$ and $n_{\mathrm{e}} = \sqrt{\varepsilon_{\mathrm{e}}}$ are the refractive indices of the crystal.

Formula (52) gives an estimate of the right side in exact equation (43), which, as expected, features a certain smallness, being quadratic in two small parameters, the anisotropy factor Δ_{e} and the ratio $\varepsilon_{\mathrm{e}}/|\varepsilon_{\mathrm{m}}|$, which are about 10^{-1} for most crystals. The first term on the right side of (52) is proportional to their product, while the second term is proportional to the anisotropy squared. Therefore, the right side in (52), and hence in (43), should be of the order of 10^{-2}, which predetermines a good convergence of the iterations.

Figure 3 shows functions $\delta s^{(1)}(\varphi)$ (52) for a group of crystals selected due to their enhanced anisotropy, i.e., the largest difference between the permittivity values ε_{o} and ε_{e} (Table 1). The values ε_{o} and ε_{e} are taken for crystals, except for calomel (Hg_2Cl_2) and sodium nitrate ($NaNO_3$), from reference book [32]. The parameters for $NaNO_3$ are reported in [22], and for Hg_2Cl_2, the data from [33, 34] are used. All data refer to the wavelength $\lambda_{\mathrm{vac}} = 0.75$ μm, similar to $\varepsilon_{\mathrm{m}} = -20.148$ for gold [31].

For negative crystals, all dependences $\delta s^{(1)}(\varphi)$ displayed in Fig. 3 monotonically decrease in the interval $0 \leqslant \varphi \leqslant \pi/2$. In the case of positive crystals, the $\delta s^{(1)}(\varphi)$ functions behave differently. In cinnabar (HgS), a monotonic increase in $\delta s^{(1)}(\varphi)$ occurs over the entire interval $0 \leqslant \varphi \leqslant \pi/2$. For the other three positive crystals shown in Fig. 3a, these functions first increase, reach a maximum, and break off on the decline branch at certain azimuths. We have already encountered a

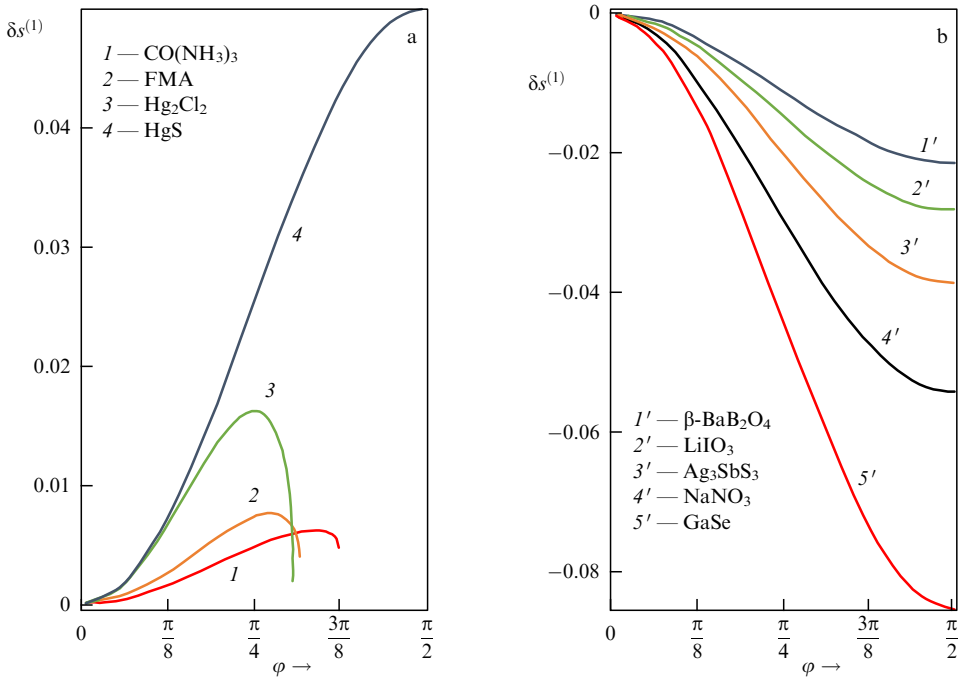

Figure 3. Dependences $\delta s^{(1)}(\varphi)$ for some positive (a) and negative (b) crystals.

similar situation in Section 4, where restrictions on the region of existence of a plasmon polariton in a negative $NaNO_3$ crystal occurred at inclination angles of the optical axis that exceeded the critical angle θ_c, at which $q_o = 0$. The physical meaning of the boundary angles φ_c in positive crystals is quite similar: in this case, these are the angles at which $q_e(\varphi_c) = 0$. We return to this aspect of the problem below. Here, of more importance for us is another feature of the curves shown in Fig. 3.

The expected smallness of their maximum values in comparison with the constant component $s^{(0)}$, which corresponds to the orientation $\varphi = 0$ and is determined by the exact formula (44), is confirmed. Table 1 shows the absolute values of $|\delta s^{(1)}|_{max}$ and their relative value $|\delta s^{(1)}|_{max}/s^{(0)}$ for ten crystals. The set of four positive crystals presented in Fig. 3a is extended in the table by adding a superanisotropic model photonic crystal (Ph Cr), considered in [18, 19, 35]. In almost all cases, the inequality $|\delta s^{(1)}_{max}| \ll s^{(0)}$ can be observed. Based on this, for some crystals presented in Table 1, even the zero approximation $s \approx s^{(0)} = \text{const}$ is a fairly acceptable estimate. The last column of the table contains the maximum deviations of functions $s^{(1)} = s^{(0)} + \delta s^{(1)}(\varphi)$ (normalized by $s^{(0)}$) from the numerically found solution $s(\varphi)$ of exact equation (43). It can be seen that for most crystals the relative error of the first approximation does not exceed 1%, and the maximum deviations occur for HgS (1.9%), $NaNO_3$ (2.2%), and GaSe (2.3%) crystals. In the case of a model photonic crystal, the situation is special. Due to the anomalous anisotropy, an acceptable accuracy ($\sim 1.7\%$) can only be achieved for this crystal after the second iteration.

Thus, as expected, even the first correction $\delta s^{(1)}$ (52) to the zeroth approximation $s^{(0)}$ (44) may be sufficient to characterize the plasmon-polariton parameters. However, as the example of the photonic crystal shows, the approximate solution $\delta s^{(1)}$ can, if required, be refined by recursive calculations in the next iterations, when the result of the kth approximation substituted into the right side of Eqn (43), taken at $\kappa_o = \kappa_o^{(k)}$ and $\kappa_e = \kappa_e^{(k)}$, gives the next, $(k+1)$th, approximation for s.

Substituting $s = s^{(0)} + \delta s^{(1)}$ into (5), in the same approximation we find

$$n^{(1)} = \sqrt{\frac{\varepsilon_o}{s^{(0)} + \delta s^{(1)}}} \approx n^{(0)}\left(1 - \frac{\delta s^{(1)}}{2s^{(0)}}\right). \tag{53}$$

Next, by analogy, we obtain

$$q_o^{(1)} = \sqrt{1 - s^{(0)} - \delta s^{(1)}}, \tag{54}$$

$$q_e^{(1)} = \sqrt{\frac{\varepsilon_e}{\varepsilon_o}(B - s^{(0)} - \delta s^{(1)})}, \tag{55}$$

$$q_m^{(1)} = \sqrt{1 - \frac{\varepsilon_m}{\varepsilon_o}(s^{(0)} + \delta s^{(1)})}. \tag{56}$$

Taking into account these values, it is easy to obtain from (46) the refined values of the parameters $\kappa_o^{(1)}$ and $\kappa_e^{(1)}$ in the next approximation:

$$\kappa_o^{(1)} \approx \kappa_o^{(0)}\left(1 - \frac{\delta s^{(1)}}{2(q_o^{(0)})^2}\right), \tag{57}$$

$$\kappa_e^{(1)} \approx \sqrt{1 - \frac{c_t^2 \Delta_e}{(q_o^{(0)})^2}(1 + \eta^{(0)})}. \tag{58}$$

The value $\kappa_e^{(1)}$ differs from $\kappa_e^{(0)}$ (49) by the addition of a small function $\eta^{(0)}$ (50) in the radicand. These values can be used to build the next iteration for $\eta^{(1)}$ and $s^{(2)}$.

Figure 4 compares the results of the analysis in the first two approximations, i.e., solutions $s^{(1)}(\varphi)$ and $s^{(2)}(\varphi)$, with a numerical solution $s(\varphi)$ of exact initial equation (43) for a positive HgS crystal and a negative GaSe crystal, whose first-approximation errors displayed in the last column of Table 1

Table 1. Material and physical parameters for 10 crystals at $\lambda_{\text{vac}} = 0.75$ μm using data [18, 28–30] and formulas (41) and (49).

	ε_{o}	ε_{e}	Δ_{e}	$s^{(0)}$	$\lvert\delta s^{(1)}\rvert_{\max}$	$\frac{\lvert\delta s^{(1)}\rvert_{\max}}{s^{(0)}}$	$\frac{\lvert s^{(1)} - s\rvert_{\max}}{s^{(0)}}$
$CO(NH_2)_2$ Carbamide	2.180	2.550	0.145	0.876	0.0065	0.74%	0.35%
2-furyl methacrylic anhydride	2.643	3.446	0.233	0.835	0.0075	0.90%	0.46%
Hg_2Cl_2 Calomel	3.771	6.566	0.426	0.718	0.0148	2.06%	0.75%
HgS Cinnabar	7.811	9.626	0.189	0.551	0.0499	9.06%	1.91%
Ph Cr Photonic crystal	2	7.5	0.733	0.702	0.0631	8.97%	$s^{(1)} \to s^{(2)}$ $15.1 \to 1.7\%$
β-BaB_2O_4 β-barium borate	2.763	2.389	−0.156	0.880	0.0210	2.39%	0.45%
$LiIO_3$ Lithium iodate	3.499	2.984	−0.173	0.849	0.0278	3.27%	0.59%
Ag_3SbS_3 Pyrargyrite	10.202	9.168	−0.113	0.529	0.0381	7.20%	0.38%
$NaNO_3$ Sodium nitrate	2.512	1.781	−0.410	0.909	0.0537	5.9%	2.2%
GaSe Gallium selenide	8.255	6.413	−0.287	0.660	0.0846	12.82%	2.27%

are the largest among real crystals. The calculations again refer to the wavelength $\lambda_{\text{vac}} = 0.75$ μm. It can be seen that in both cases all the curves originate from the same point, corresponding to the exact solution at $\varphi = 0$, $s(0) = s^{(0)}$ (44), and then rise (Fig. 4a) or fall (Fig. 4b) following close trajectories. The deviations of the approximate solutions from the exact one are the largest on the right edge, where they amount, compared with $s^{(0)}$, in the first and second order, respectively, to $\sim 1.9\%$ and 1% for cinnabar and $\sim 2.3\%$ and 0.18% for gallium selenide. As can be seen from Table 1, these figures for a photonic crystal are $\sim 15\%$ and 1.7%.

We now return to Fig. 3a, where for three (out of four positive) crystals, the region where the solution exists turns out to be limited from above by the critical azimuth φ_{c}, at which $q_{\text{e}} = 0$. If the angle φ_{c} is exceeded, the parameter $q_{\text{e}}(\varphi)$

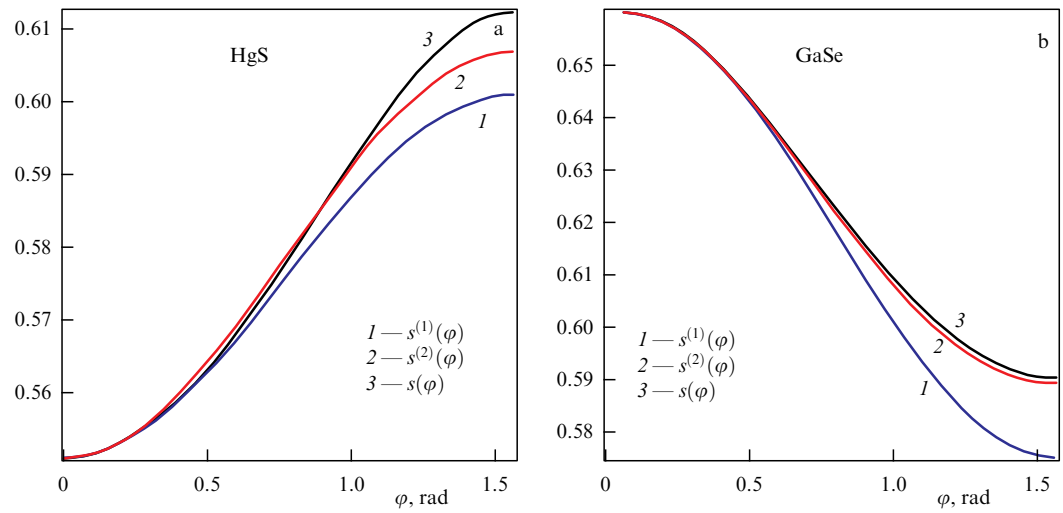

Figure 4. Comparison of approximate curves *1* — $s^{(1)}(\varphi)$ and *2* — $s^{(2)}(\varphi)$ that correspond to the first and second iteration, respectively, with curve *3* — $s(\varphi)$ being the numerical solution of Eqn (22) for HgS (a) and GaSe (b) crystals.

Table 2. Comparison of angles $\varphi_c^{(0)}$, $\varphi_c^{(1)}$, $\varphi_c^{(2)}$, and φ_c for four crystals.

	$\varphi_c^{(0)}$	$\varphi_c^{(1)}$	$\varphi_c^{(2)}$	φ_c
$CO(NH_2)_2$	67.77°	65.39°		63.28°
FMA	57.34°	56.38°		55.74°
Hg_2Cl_2	56.09°	56.00°		55.85°
Ph Cr	39.6°	44.6°	52.1°	53.02°

becomes imaginary, which corresponds to the transformation of an extraordinary localized partial mode in superposition (2) into a bulk wave propagating at an angle to the interface surface with energy diversion deep into the crystal, so the polariton becomes a leaky mode. Thus, the region where the localized eigenmode under study exists turns out to be limited by the interval $0 \leqslant \varphi \leqslant \varphi_c$. In the particular case under consideration here, $c_{\mathbf{n}} = 0$, the exact critical angle φ_c is found from the equation

$$\sin\varphi_c = \left[\Delta_e\left(1 - \frac{\varepsilon_m(2 - \varepsilon_m/\varepsilon_e)}{\varepsilon_e(1 - \varepsilon_m/\varepsilon_o)}\right)\right]^{-1/2} \leqslant 1\,. \tag{59}$$

We now compare for these three crystals and the photonic crystal in Table 1 exact solutions φ_c of Eqn (59) with the approximate values $\varphi_c^{(0)}$ and $\varphi_c^{(1)}$ that follow from equations $q_e^{(0)}(\varphi) = 0$ (48) and $q_e^{(1)}(\varphi) = 0$ (55). The results of this comparison, displayed in Table 2, are fairly optimistic for real crystals, even in the zeroth approximation, not to mention the first iteration (the second iteration was not calculated). As for the model anisotropic photonic crystal, to get closer to the exact value, the second iteration was again required.

It is noteworthy that, when passing from the parameter s to the physical parameters n and $q_{o,e,m}$, the approximation error becomes even smaller due to the presence of the correction $\delta s^{(1)}$ in the radicand in Eqns (53)–(56). This is shown in Fig. 5, which compares the approximate functions $n^{(1)}(\varphi)$, $q_{o,e,m}^{(1)}(\varphi)$ with the corresponding numerical solutions of exact equations (5) and (43) for HgS and GaSe crystals.

Figure 5 shows that the largest deviation, which is observed between the $n(\varphi)$ curves in the GaSe crystal, amounts to a relative value of 1.4% at $\varphi = \pi/2$. No deviations in any other curve in both crystals exceed 1%. If plotted on a normal scale without breaks in the ordinate axis, as in Fig. 5, all the compared pairs of curves, except for $n(\varphi)$, merge: the gap between them becomes smaller than the line thickness. The $n(\varphi)$ curves become approximately four times closer.

The intersection of curves $q_o(\varphi)$ and $q_e(\varphi)$ in Fig. 5 for both crystals, HgS and GaSe, should also be noted. We find the exact positions of these points analytically. It follows from (5) that, in the plane under consideration ($c_{\mathbf{n}} = 0$, $A = 1$), the intersection occurs at $q_o(\varphi) = q_e(\varphi) = |c_{\mathbf{t}}| = \sin\varphi$, $s = \cos^2\varphi$. Substitution of these values into the dispersion equation (40) determines the searched for position of the intersection point φ_{deg}:

$$\cot\varphi_{deg} = 2\sqrt{\frac{\varepsilon_o\left(|\varepsilon_m| + \varepsilon_e\right)\left(|\varepsilon_m| - \varepsilon_o\right)}{(\varepsilon_o + \varepsilon_e)^2\left(|\varepsilon_m| + \varepsilon_o\right)}}\,. \tag{60}$$

Figure 5 shows that the approximate theory yields the positions of intersection points close to exact values (60).

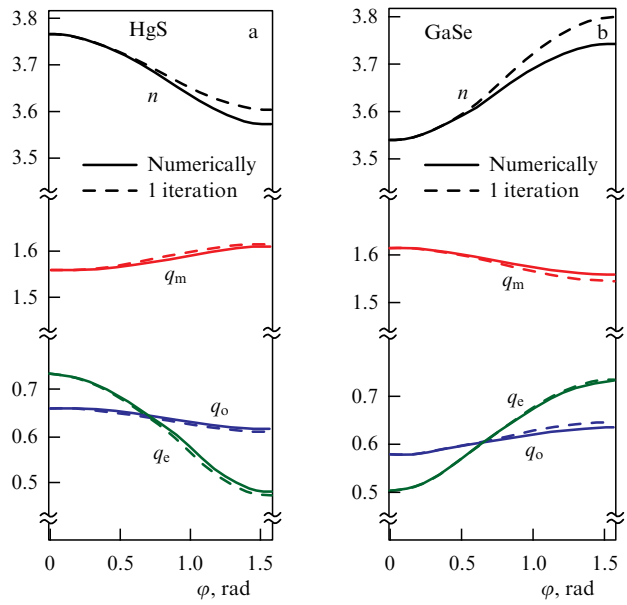

Figure 5. Comparison of functions $n(\varphi)$ and $q_{o,e,m}(\varphi)$ found numerically from exact equations (5) and (43) (solid curves) with their first-approximation solutions (53)–(56) (dashed curves) for HgS – Au (a) and GaSe – Au (b) interfaces at $\lambda_{vac} = 0.75$ μm.

It can be easily checked that, when moving towards the point φ_{deg}, it is not only localization parameters of the ordinary and the extraordinary components but also polarization vectors (3) that come close. The degenerate waves propagating in this direction are referred to as Dyakonov–Voigt plasmon-polaritons. They feature fairly nontrivial properties that require a special description [36, 37], which is beyond the scope of this study. It is only worth noting that the partial waves of the degenerate polariton in a crystal have coinciding polarization parameters but different vector amplitudes. One polariton component features a circular polarization and a scalar amplitude that linearly increases as the distance from the interface grows.

Thus, comparisons of the approximated solution with exact ones in Figs 4 and 5 and Tables 1 and 2 indicate that the procedure proposed in this section to analytically describe the plasmon-polariton in the Dyakonov geometry proved to be fairly successful. For all 'live' crystals, including most anisotropic ones, the first iteration provides a fairly high accuracy of description. It is for the model superanisotropic crystal alone that refinement was needed, but, in this case as well, the second iteration was sufficient. The next section presents a generalization of the described approach for an arbitrary geometry.

6. Generalization of the iteration formalism for the case of arbitrary orientation

General equation (22) now contains all components of the vector $\mathbf{c}$, and hence both functions $A(c_{\mathbf{n}})$ and $B(c_{\mathbf{t}})$ (6) that are different from unity. We solve this equation by analogy with Section 5. Therefore, it is convenient to write it in a form that generalizes Eqn (43),

$$s - s_A^{(0)} = c_{\mathbf{t}}^2\Delta_e\left\{\frac{\varepsilon_e}{\varepsilon_e - \varepsilon_m} - \frac{\kappa_o - 1}{\kappa_o + \bar{\kappa}_e}\right\}\chi\,, \tag{61}$$

where the parameter κ_o is determined as before by Eqn (46) and new notations are introduced:

$$s_A^{(0)} = \frac{1 - \varepsilon_o \varepsilon_e / \varepsilon_m^2}{A - \varepsilon_e/\varepsilon_m}\,, \tag{62}$$

$$\bar{\kappa}_e = -\frac{A q_e \varepsilon_m}{q_m \varepsilon_e}\,, \qquad \chi = \frac{1 - \varepsilon_e/\varepsilon_m}{A - \varepsilon_e/\varepsilon_m}\,. \tag{63}$$

It should be stressed that the obtained new form of Eqn (61) is exact and fully equivalent to initial equation (22).

We now show that the right part of Eqn (61) is again fairly small in comparison with the terms in the left part. Given this circumstance, the iteration method can also be applied to solve Eqn (61). In the zeroth order, we can set $s = s_A^{(0)}$ (62), which formally agrees with our solution (33), which described in Section 4 the particular case $\varphi = 0$. In the same zeroth approximation, taking into account (5), we obtain

$$q_o^{(0)} = \sqrt{1 - \frac{1 - \varepsilon_o \varepsilon_e/\varepsilon_m^2}{A - \varepsilon_e/\varepsilon_m}}\,, \tag{64}$$

$$q_e^{(0)} = \frac{1}{A}\sqrt{\frac{\varepsilon_e}{\varepsilon_o}\left(\frac{1 - A\varepsilon_o/\varepsilon_m}{1 - A\varepsilon_m/\varepsilon_e} - c_{\mathbf{t}}^2 \Delta_e\right)}\,, \tag{65}$$

$$q_m^{(0)} = \sqrt{\frac{A - \varepsilon_m/\varepsilon_o}{A - \varepsilon_e/\varepsilon_m}}\,. \tag{66}$$

Substituting Eqns (64)–(66) into the formulas for κ_o (46) and $\bar{\kappa}_e$ (63), we also find the parameters

$$\kappa_o^{(0)} \approx \sqrt{\frac{\varepsilon_e}{\varepsilon_o} - \frac{c_{\mathbf{n}}^2 \Delta_o \varepsilon_m/\varepsilon_o}{1 - \varepsilon_o/\varepsilon_m}}\,, \qquad \bar{\kappa}_e^{(0)} = \sqrt{1 - c_{\mathbf{t}}^2 \Delta_e \frac{1 - A\varepsilon_m/\varepsilon_e}{1 - A\varepsilon_o/\varepsilon_m}}\,. \tag{67}$$

In deriving the first formula in (67), terms of the second order of smallness, like $(\varepsilon_{e,o}/\varepsilon_m)^2$ and $\Delta_o(\varepsilon_o/\varepsilon_m)$, were omitted. Based on this, a step to the next iteration, the first order approximation, can be made:

$$s^{(1)} = s_A^{(0)}(\theta) + \delta s_A^{(1)}(\theta, \varphi)\,, \tag{68}$$

where

$$\delta s_A^{(1)} = \Delta_e c_{\mathbf{t}}^2(\theta) \chi(\theta) \eta_A^{(0)}(\theta, \varphi)\,, \tag{69}$$

$$\eta_A^{(0)} = \frac{\varepsilon_e}{\varepsilon_e - \varepsilon_m} - \frac{\kappa_o^{(0)}(\theta) - 1}{\kappa_o^{(0)}(\theta) + \bar{\kappa}_e^{(0)}(\theta, \varphi)}\,. \tag{70}$$

Similar to Section 5, the iterative procedure under development ensures rapid convergence only provided the right side of Eqn (61) is fairly small. Analysis shows that the estimate $\delta s_A^{(1)}(\theta, \varphi)$ (69) found in the first order is actually small for most crystals for all angles φ and θ within the region where the plasmon-polariton exists. It should be noted here that the possible reversion of signs of the radicands in Eqn (67) (as in (5)) is of no concern, since it would only indicate going beyond the regions of existence. In frames of simple limiting consideration, for small θ ($c_{\mathbf{n}}^2 \ll 1$) the analysis in Section 5 based on Eqn (52) can be repeated. At large θ, a new additional small factor emerges, $c_{\mathbf{t}}^2 \ll 1$, so in the limit $\delta s_A^{(1)}(\pi/2, \varphi) = 0$. For intermediate orientations, all three small factors are operative: $c_{\mathbf{t}}^2 \Delta_e \eta_A^{(0)}$. It is shown below in an alternative approach.

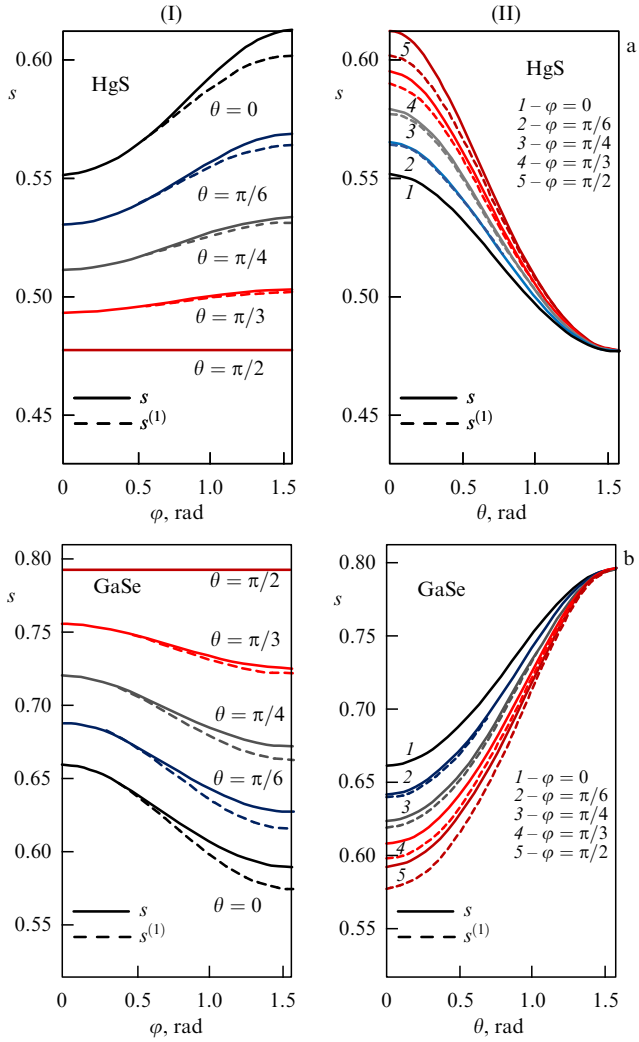

Figure 6. Comparison of first-approximation functions $s^{(1)}(\theta, \varphi)$ (67) with numerical solutions $s(\theta, \varphi)$ of exact equation (60) for HgS (a) and GaSe (b) crystals; $\lambda_{vac} = 0.75$ μm.

It is natural to compare the results of the approximate analysis based on Eqns (68)–(70) with the numerical solution $s(\theta, \varphi)$ of exact equation (61) for the same pair of crystals for which the largest deviations were found in Section 5. Figure 6 displays such a comparison for these crystals: for positive cinnabar (Fig. 6a) and negative gallium selenide (Fig. 6b). Pairs of curves $s^{(1)}(\varphi)$ and $s(\varphi)$ were plotted for a series of five angles, $\theta = 0, \pi/6, \pi/4, \pi/3$, and $\pi/2$ (I), and pairs, $s^{(1)}(\theta)$ and $s(\theta)$, for fixed azimuths $\varphi = 0, \pi/6, \pi/4, \pi/3$, and $\pi/2$ (II). If $\theta = \pi/2$, when the optical axis **c** is orthogonal to the interface, which thereby becomes the transverse isotropy plane, the function $s(\pi/2, \varphi)$ naturally becomes independent of the azimuth φ. Formally, in this case, the identity $c_{\mathbf{t}}(\pi/2, \varphi) \equiv 0$ is valid, so Eqns (62) and (69) automatically yield the same exact solution: $s = s_A^{(0)}(\pi/2) = \text{const}$, which can be seen in Fig. 6(I). In negative crystals, this constant turns out to be the absolute maximum of the function $s(\theta, \varphi)$, and, in positive crystals, its absolute minimum (see Fig. 6(II)).

As the angle θ decreases, the width of the region of variation of the function $s(\varphi)$, estimated using the value $|\delta s^{(1)}|_{max}$, monotonically grows. Concurrently, the deviation between curves $s^{(1)}(\varphi)$ and $s(\varphi)$ also grows to reach a maximum at $\theta = 0$, $\varphi = \pi/2$: 1.9% for HgS and 2.3% for

Table 3. Maximal relative differences of functions $s^{(1)}(\varphi)$ and $s(\varphi)$ for various θ.

θ, rad		0	$\pi/6$	$\pi/4$	$\pi/3$	$\pi/2$
$\dfrac{\lvert s^{(1)} - s\rvert_{\max}}{s_A^{(0)}(\pi/2)}$	HgS	1.9%	0.94%	0.39%	0.12%	0
	GaSe	2.3%	1.8%	1.2%	0.49%	0

GaSe (see Table 1). Thus, the testing of the first approximation under discussion, which was carried out in Section 5 specifically for $\theta = 0$, seems to be sufficient. Figure 6(I) shows that an increase in θ only reduces the already small errors in our approximation (Table 3). It should be added that the differences among the solutions displayed in Fig. 6 refer to crystals with a uniquely high anisotropy and can be significantly reduced in the next iteration (see Fig. 4). As can be seen from Table 1, for the vast majority of crystals, the errors in even the first-approximation solutions do not exceed 1%.

7. Conclusion

One of the key results of this study is the obtained explicit form of real dispersion equation (22) (see Section 3), the solutions of which determine the main properties of the plasmon-polariton at interface orientations that allow its existence for given material parameters. These properties are described above analytically for a number of orientations, including an arbitrary one, on the basis of an exact analysis (see Section 4) or in an approximate way, based on the iterative formalism developed in Sections 5 and 6.

Attention should be paid here to a 'technical' detail underlying the surprisingly fast convergence of the mentioned iterative formalism used in Sections 5 and 6. It should be recalled that we used in our analysis four forms of the exact dispersion equation: (22), (40), (43), and (61). It can be easily seen that the first two equations, (22) and (40), contain on their right side an anisotropy parameter, which, generally speaking, is not too small, $\Delta_e \sim 10^{-1}$. However, the last two forms, (43) and (61), obtained by transformation, the concept of which is described below Eqn (40), contain a really small factor of $\sim 10^{-2}$ on the right side, the estimate of which is given in Eqns (52) and (69) and Table. 1. It is this factor that governs the effectiveness of the iterative procedure we have proposed.

The analytical theory developed in this study makes it possible to describe the dependences of the wave parameters of the plasmon-polariton on the orientation of the interface and material constants. As we have seen, the higher the crystal anisotropy, the more diverse the wave pattern. Under certain conditions, a polariton in a crystal can even lose its localization, i.e., it becomes a bulk one.

Here, it is reasonable to consider for comparison the opposite limiting case of the complete loss of anisotropy, when the crystal transforms into an isotropic dielectric medium. In this limiting case, $\varepsilon_e \to \varepsilon_o$, $\Delta_{e,o} = 0$, $A = B = 1$, $q_e \to q_o$, and dispersion equation (22) is greatly simplified to

$$\varepsilon_m q_o + \varepsilon_o q_m = 0\,. \tag{71}$$

This shows that, if $\varepsilon_m > 0$, i.e., when metal is replaced by a normal isotropic dielectric, dispersion equation (71) has no solutions, as already stated in the introduction. It is only if $\varepsilon_m < 0$, i.e., in cases of a plasmon-polariton or a dispersive polariton, that the terms on the left side of Eqn (71) turn out to be of opposite signs, so that it has a simple solution:

$$s = 1 - \frac{\varepsilon_o}{|\varepsilon_m|}\,. \tag{72}$$

Consequently, we obtain from (5) in the same limit

$$q_o = \sqrt{\frac{\varepsilon_o}{|\varepsilon_m|}}\,, \qquad q_m = \sqrt{\frac{|\varepsilon_m|}{\varepsilon_o}}\,. \tag{73}$$

If $\varepsilon_e = \varepsilon_o$, the same formulas (72) and (73) follow, of course, from Eqns (33)–(36). By analogy with the analysis carried out in Section 4, the requirement $s > 0$ limits the domain of existence by the criterion

$$|\varepsilon_m| > \varepsilon_o\,. \tag{74}$$

As in Section 4, this criterion is definitely of no practical interest due to a more serious physical limitation on the value of $|\varepsilon_m|$ associated with plasmon damping in the metal. For a plasmon-polariton to exist, it is necessary that its path L significantly exceed its own wavelength: $L \gg \lambda$. This requires a paradoxical increase in λ with a transition to the infrared region (L grows faster than λ). In this frequency range, the growth of L is provided by a sharp increase in $|\varepsilon_m|$ [21, 31], so that the very existence of a plasmon-polariton guarantees the fulfillment of inequality (74).

However, even with this choice of λ, the typical free path of a plasmon-polariton is usually several ten micrometers. Therefore, in plasmonics, the problem of increasing the path length persists. One of the effective ways to solve this problem is to straightforwardly replace an isotropic dielectric with a crystal [19–21]. In particular, our study [21] has shown that the choice of interface orientation corresponding to a weakly localized (quasi-bulk) polariton in a crystal should sharply increase the free path of the plasmon-polariton. An increase in the free path is expected to be approximately proportional to the ratio of the energy fluxes carried by the polariton and plasmon.

In Section 5, exact formula (59) for the Dyakonov geometry is obtained, which specifically determines the critical orientation in which the bulk polariton of the extraordinary partial branch ($q_e = 0$) is realized in the crystal. Table 2, presented in the same section, shows the corresponding critical angles φ_c for four positive crystals. Study [21] has shown for two of these crystals that the free path L of the plasmon-polariton sharply increases by several orders of magnitude as the orientation approaches the critical one $\varphi \to \varphi_c$, shown in [21].

It should be noted that bulk polaritons also exist in biaxial crystals adjoining a metal [38]; therefore, the noted well-pronounced effect can also occur in dielectrics of arbitrary anisotropy. However, in a similar semi-limited isotropic dielectric, delocalization of a polariton is not possible; therefore, this effect is purely anisotropic.

This study was supported by the Ministry of Science and Higher Education of the Russian Federation as part of the state assignment to the Federal Research Center Crystallography and Photonics of the Russian Academy of Sciences.

References

1. Landau L D, Lifshitz E M *Electrodynamics of Continuous Media* (Oxford: Pergamon Press, 1984); Translated from Russian: *Elektrodinamika Sploshnykh Sred* (Moscow: Nauka, 1982)
2. Barnett D M, Lothe J *Proc. R. Soc. Lond. A* **402** 135 (1985)

3. Agranovich V M *Sov. Phys. Usp.* **18** 99 (1975); *Usp. Fiz. Nauk* **115** 199 (1975)
4. Agranovich V M *Sov. Phys. Usp.* **23** 420 (1980); *Usp. Fiz. Nauk* **131** 513 (1980)
5. Agranovich V M, Mills D L (Eds) *Surface Polaritons: Electromagnetic Waves at Surfaces and Interfaces* (Amsterdam: North-Holland, 1982); Translated from Russian: *Poverkhnostnye Polyaritony. Elektromagnitnye Volny na Poverkhnostyakh i Granitsakh Razdela* (Moscow: Nauka, 1985)
6. Alshits V I, Lyubimov V N *J. Exp. Theor. Phys.* **101** 779 (2005); *Zh. Eksp. Teor. Fiz.* **128** 904 (2005)
7. D'yakonov M I *Sov. Phys. JETP* **67** 714 (1988); *Zh. Eksp. Teor. Fiz.* **94** 1194 (1988)
8. Walker D B, Glytsis E N, Gaylord T K *J. Opt. Soc. Am. A* **15** 248 (1998)
9. Alshits V I, Lyubimov V N *Phys. Solid State* **44** 386 (2002); *Fiz. Tverd. Tela* **44** 371 (2002)
10. Alshits V I, Lyubimov V N *Phys. Solid State* **44** 1988 (2002); *Fiz. Tverd. Tela* **44** 1895 (2002)
11. Cojocaru E *J. Opt. Soc. Am. A* **32** 782 (2015)
12. Zhou C, Mackay T G, Lakhtakia A *Sci Rep.* **10** 12894 (2020)
13. Zayats A V, Smolyaninov I I, Maradudin A A *Phys. Rep.* **408** 131 (2005)
14. Maier S A *Plasmonics: Fundamentals and Applications* (New York: Springer, 2007)
15. Polo J A (Jr.), Lakhtakia A *Laser Photon. Rev.* **5** 234 (2011)
16. Takayama O et al. *Electromagnetics* **28** 126 (2008)
17. Abdulhalim I *J. Opt. A* **11** 015002 (2009)
18. Zhang T, Shan F *J. Nanomater.* **2014** 495381 (2014)
19. Krokhin A A, Neogi A, McNeil D *Phys. Rev. B* **75** 235420 (2007)
20. Nagaraj, Krokhin A A *Phys. Rev. B* **81** 085426 (2010)
21. Alshits V I, Lyubimov V N *JETP Lett.* **112** 127 (2020); *Pis'ma Zh. Eksp. Teor. Fiz.* **112** 127 (2020)
22. Depine R A, Gigli M L *Opt. Lett.* **20** 2243 (1995)
23. Depine R A, Gigli M L *J. Opt. Soc. Am. A* **14** 510 (1997)
24. Liscidini M, Sipe J E *Phys. Rev. B* **81** 115335 (2010)
25. Alshits V I, Lyubimov V N *J. Exp. Theor. Phys.* **111** 591 (2010); *Zh. Eksp. Teor. Fiz.* **138** 669 (2010)
26. Stroh A N *J. Math. Phys.* **41** 77 (1962)
27. Galynsky V M, Furs A N, Barkovsky L M *J. Phys. A* **37** 5083 (2004)
28. Li R et al. *Appl. Phys. Lett.* **92** 141115 (2008)
29. Liu H-H, Chang H *IEEE Photon. J.* **5** 4800806 (2013)
30. Alshits V I, Lyubimov V N, Nowacki J P, Drabik A *Int. J. Appl. Electromagn. Mech.* **64** 879 (2020)
31. Johnson P B, Christy R W *Phys. Rev. B* **6** 4370 (1972)
32. Dmitriev V G, Gurzadyan G G, Nikogosyan D N *Handbook of Nonlinear Optical Crystals* (Berlin: Springer, 1999)
33. Konstantinova A F et al. *Opticheskie Svoistva Kristallov* (Optical Properties of Crystals) (Minsk: Navuka i Tekhnika, 1995)
34. Perekalina Z B et al. *Opt. Spectrosc.* **42** 653 (1977); *Opt. Spektrosk.* **42** 1134 (1977)
35. Halevi P, Krokhin A A, Arriaga J *Phys. Rev. Lett.* **82** 719 (1999)
36. Marchevskii F N, Strizhevskii V L, Strizhevskii S V *Sov. Phys. Solid State* **26** 911 (1984); *Fiz. Tverd. Tela* **26** 1501 (1984)
37. Zhou C, Mackey T G, Lakhtakia A *Phys. Rev. A* **100** 033809 (2019)
38. Alshits V I, Lyubimov V N *Crystallogr. Rep.* **54** 941 (2009); *Kristallografiya* **54** 989 (2009)